A Branched Kinetic Scheme Describes the Mechanochemical Coupling of Myosin Va Processivity in Response to Substrate

Chong Zhang,[†] M. Yusuf Ali,[†] David M. Warshaw,[†*] and Neil M. Kad[‡*]
[†]Department of Molecular Physiology and Biophysics, University of Vermont, Burlington, Vermont; and [‡]School of Biological Sciences, University of Essex, Colchester, United Kingdom

ABSTRACT Myosin Va is a double-headed cargo-carrying molecular motor that moves processively along cellular actin filaments. Long processive runs are achieved through mechanical coordination between the two heads of myosin Va, which keeps their ATPase cycles out of phase, preventing both heads detaching from actin simultaneously. The biochemical kinetics underlying processivity are still uncertain. Here we attempt to define the biochemical pathways populated by myosin Va by examining the velocity, processive run-length, and individual steps of a Qdot-labeled myosin Va in various substrate conditions (i.e., changes in ATP, ADP, and P_i) under zero load in the single-molecule total internal reflection fluorescence microscopy assay. These data were used to globally constrain a branched kinetic scheme that was necessary to fit the dependences of velocity and run-length on substrate conditions. Based on this model, myosin Va can be biased along a given pathway by changes in substrate concentrations. This has uncovered states not normally sampled by the motor, and suggests that every transition involving substrate binding and release may be strain-dependent.

INTRODUCTION

Myosin Va is a double-headed molecular motor that transports cargo in eukaryotic cells (1,2). With its movement powered by ATP hydrolysis, myosin Va walks processively along actin tracks, taking 36-nm hand-over-hand steps (3–8). Myosin Va's processivity, the ability to undergo multiple displacement-generating ATPase cycles without dissociating from its track, is due in part to the large fraction of its actin-activated ATPase cycle spent strongly bound to actin (i.e., high duty ratio) (9,10). With the motor's ATPase activity being rate-limited by ADP release (4), the probability is high that at least one head will be tightly bound to actin at any point in time. To increase this probability further, interhead communication must exist to ensure that the ATPase cycles remain out of phase, preventing simultaneous detachment of both heads. This communication is mediated by interhead strain, which may slow ADP release from the leading head (11–13) while accelerating ADP release from the trailing head (11,14), thus biasing the motor to take a forward step.

Although the biochemistry and mechanics of processive movement are reasonably well defined, their integration into a precise mechanochemical model during a processive run presents numerous challenges. Previous studies have suggested that myosin Va utilizes a single biochemical pathway (14,15), whereas others have proposed branched kinetic schemes (16–19). In this study, we do not, a priori, define pathways through a model; instead, we have simply defined the possible states that each head may occupy as the two heads undergo their gated, actin-activated ATPase cycles. To determine the most likely kinetic scheme through these various states, we have made single molecule processivity measurements (i.e., velocity and run-length) across a range of substrate conditions (i.e., ATP, ADP, P_i), assuming that such changes would probe specific states in the mechanochemical cycle by forcing the motor to take alternate biochemical pathways. Combined with data from the literature, we were able to globally constrain this multistate scheme, with the model outcome suggesting that myosin Va utilizes three distinct but interrelated biochemical pathways during cargo transport. Alterations in substrate conditions can redistribute the biochemical flux through these pathways while maintaining processive motion. Furthermore, comparison of model rate constants for biochemical transitions involving P_i-release, ADP-release, and ATP-binding at different states in the processive cycle indicates that intramolecular strain generated between the two heads can modulate these specific transition rates. Although we test the unloaded molecule, it is possible that our approach could offer the potential to unify much of what we know about myosin Va's mechanochemistry into one testable model.

MATERIALS AND METHODS

Myosin motor construct and data acquisition

All experiments were performed using double-headed murine heavy meromyosin Va N-terminally tagged with biotin (myosin Va). Measures of single motor processivity (i.e., velocity, run-length, and step size) were characterized under varying substrate conditions (i.e., ATP, ADP, and P_i) in high salt (100 mM KCl) actin buffer at room temperature (25 ± 1°C) (see the Supporting Material).

Myosin Va was fluorescently tagged by conjugation of its biotin moiety with a single 655-nm emitting streptavidin-Qdot and its movement recorded on a custom-built total internal reflection fluorescence microscope (see the Supporting Material for more details). The acquisition was adjusted

Submitted June 26, 2012, and accepted for publication July 17, 2012.

*Correspondence: nkad@essex.ac.uk or david.warshaw@uvm.edu

Editor: E. Ostap.

0006-3495/12/08/0728/10 $2.00

http://dx.doi.org/10.1016/j.bpj.2012.07.033

to an appropriate frame rate for each solution condition so that the myosin displacement between frames was ~0.1 μm. The total observation time per flowcell was ~15 min, during which no systematic changes to the velocity were noted.

Data analysis

Run-length and velocity

Analysis of myosin Va movement was performed using the routine MtrackJ (ImageJ plugin; National Institutes of Health, Bethesda, MD)); only runs longer than 0.5 μm that visibly terminated before reaching the end of an actin filament were analyzed. These criteria, although eliminating short apparent runs associated with Qdots that diffuse in and out of the image plane, do contribute to a systematic run-length underestimation by limiting the maximum possible run-length to that of the actin filament length. However, to minimize this error we only analyzed runs on actin filaments with lengths >6 μm. We expect the degree of error to be small (<10%) because the probability of observing very long runs is small and the minimum actin length far exceeds the longest average run-length. The velocity (V) of an individual myosin Va run was determined by dividing the total distance traveled by the transit time; and the reported velocity is the mean velocity of all the individual runs in each condition. Myosin Va run-lengths were defined as the total distance traveled along an actin filament from its initial appearance to dissociation and the distribution of run-lengths was fitted to an exponential distribution by means of a cumulative frequency plot (see Fig. S1 in the Supporting Material).

Step size

Individual steps of myosin Va HMM were examined at 3 μM ATP, where the stepping rate is slow enough to be resolved at six frames/s. Each Qdot image was fitted to a two-dimensional Gaussian representing the point spread function (7), providing a resolution of 6 nm (8). Displacement of Qdots was plotted as a function of time, with steps automatically detected using a step-finding algorithm (20).

The kinetic model, optimization, and sensitivity

The branched kinetic model of Baker et al. (16) describing myosin Va's mechanochemistry under unloaded conditions serves as the starting point for our modeling efforts described here (Fig. 1). This model follows the ATPase cycle of only the trailing head and thus represents only half of the motor's ATPase activity. By explicitly assuming that ADP release is inhibited from the lead head, the biochemical cycle of the lead head waits for the trail head before beginning the exact same cycle. In making this assumption, we restrict the model to six states; without this assumption, we would necessarily include many more low probability states that would reduce the accuracy of the model by increasing its number of parameters. For this reason, the model excludes the possibility of backstepping, the probability of which is extremely low (i.e., 0.3%) under unloaded conditions (19).

Of the states, 1 and 6 are modeled as identical (i.e., there is no explicit probability of being in state 6 (P_6), only a probability of being in state 1 (P_1): see differential equations below), because ATP hydrolysis is rapid (4). States 1 and 6 differ only in that the trailing head has now become the new leading head (state 6) after its release from actin upon binding ATP (states 3 and 5) and being swung forward by the powerstroke of the former leading head (21). This results in a 36-nm step of the motor's centroid. Starting in state 1, the motor can travel down three distinct kinetic pathways. Path A (state 1→4→5→6) is traveled with P_i release from the leading head of state 1 followed by a powerstroke, preceding ADP release from the trailing head. Alternatively path B is taken (state 1→2→5→6) when ADP releases from the trailing head of state 1 first, followed by P_i release from the lead head and a powerstroke. Finally, path C (state 2→3→6) is traveled if ATP binds to the trailing head before P_i is released from the leading head of state 2.

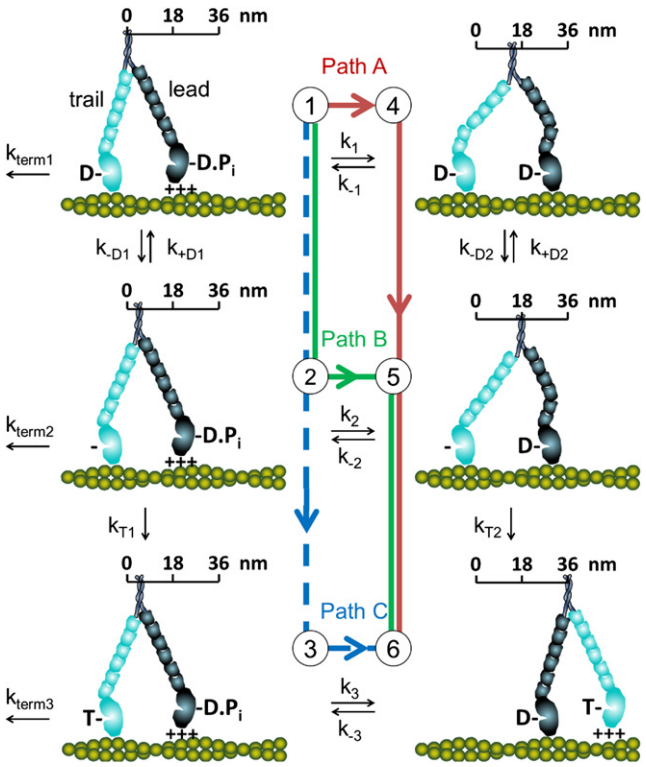

FIGURE 1 Minimal kinetic scheme to describe myosin Va's mechanochemistry. Starting from state 1, myosin Va can take path A, where P_i release from the leading head precedes ADP release from the trailing head, or path B, where ADP release from the trailing head of state 1 precedes P_i release from the leading head. Path C arises from the subdivision of path B when ATP binds the trailing head before P_i release from the leading head of state 2. State 6 is the same mechanical state as state 1 where the cycle starts again with the two heads switching roles as the leading and trailing head. States 1–3 are the three states where myosin Va may detach from actin. (Symbol +++) Weaker electrostatic association of the leading head with actin (24).

We assume that run termination can occur from any state in which the motor has only one head attached in either the strongly or weakly bound state (states 1, 2, 3). Given that states 1 and 6 are identical, state 1 has two potential paths for detachment: directly through k_{term1} or P_i-mediated through k_{term3} once P_i binds to state 6 and populates the termination prone state 3.

To determine the forward and reverse rate constants for the various transitions within the model, we fit myosin Va's velocity and run-length as a function of ATP, ADP, and P_i concentration. The model solution was based on the simple steady-state formalism described below.

The branched kinetic scheme (Fig. 1) can be solved by first describing the probabilities of being in each state as P_1 (P_6), P_2, P_3, P_4, and P_5, which are proportional to the state lifetimes, as defined by the differential equations below with the first and second-order rate constants defined in Fig. 1:

$$\frac{dP_1}{dt} = P_5\cdot k_{T2}\cdot[ATP] + P_2\cdot k_{+D1}\cdot[ADP] + P_3\cdot k_3 + P4\cdot k_{-1}\cdot[Pi] - P_1(k_1 + k_{-D1} + k_{-3}\cdot[Pi]),$$

$$\frac{dP_2}{dt} = P_1\cdot k_{-D1} + P_5\cdot k_{-2}\cdot[Pi] - P_2(k_2 + k_{+D1}\cdot[ADP] + k_{T1}\cdot[ATP]),$$

$$\frac{dP_3}{dt} = P_2 \cdot k_{T1} \cdot [ATP] + P_1 \cdot k_{-3} \cdot [Pi] - P_3 \cdot k_3,$$

$$\frac{dP_4}{dt} = P_1 \cdot k_1 + P_5 \cdot k_{+D2}[ADP] - P_4(k_{-1} \cdot [Pi] + k_{-D2}),$$

$$\frac{dP_5}{dt} = P_2 \cdot k_2 + P_4 \cdot k_{-D2} - P_5(k_{+D2} \cdot [ADP] + k_{-2} \cdot [Pi] + k_{T2} \cdot [ATP])$$

$$P_1 + P_2 + P_3 + P_4 + P_5 = 1.$$

The velocity (V) defined in this model is the ATPase rate per head times the displacement of the motor's center of mass associated with each ATPase cycle (i.e., 36 nm), where the ATPase rate equals the sum of the fluxes through all three pathways. Therefore, velocity is

$$V = 36\ \text{nm} \cdot (P_5 \cdot k_{T2} \cdot [\text{ATP}] + P_2 \cdot k_{T1} \cdot [\text{ATP}]).$$

Run-length (L) is defined as the velocity divided by the termination rate ($Term$),

$$L = \frac{V}{Term},$$

where

$$Term = P_1 k_{\text{term1}} + P_2 k_{\text{term2}} + P_3 k_{\text{term3}}.$$

The kinetic model described here by 15 parameters (i.e., forward and reverse rate constants; see Fig. 1 and Table 1) and three pathways is substantially more detailed than the simplified earlier version described in Baker et al. (16), which was defined by only eight rate constants and two pathways. The model parameters (i.e., rate constants) were estimated and optimized using MATLAB (The MathWorks, Natick, MA) to fit the run-length and velocity model predictions globally to the experimental data under various solution conditions (i.e., six velocity and run-length relationships). We fit the data in two stages:

First stage. Random numbers were chosen for all 15 parameters from within a range of starting values (Table 1, Stage No. 1 Search) that were loosely based on literature values where possible. These were chosen to limit the global search through parameter space and to prevent the search from becoming unreasonably computationally intensive. Velocities and run-lengths across the different substrate conditions were predicted using the randomly selected set of parameters; the goodness of fit to these data was then evaluated using χ^2 statistical analysis.

Second stage. After 10^9 runs, the best fitting parameters were then used as starting values for the second stage of parameter fine-tuning (Table 1, Stage No. 2 Search). In this second fine-tuning stage, each parameter was varied systematically by 200 increments within a range of 0.85-1.15 times their starting value; velocity and run-length predictions for each increment were made across the different substrate conditions while the remaining parameter values were kept constant. If the fit was improved, the new value was kept as the starting value. This process was then repeated for the next parameter and so on, to generate up to 15 new starting values. This was considered one optimization cycle. After 10^5 cycles, the parameter values remaining on the last cycle were our optimal parameter values (Table 1), which were used to generate the model predictions presented in this study.

Sensitivity of the model predictions to changes in parameter estimates was assessed by varying each value between 10 and 200% of its optimal value and then calculating the velocity and run-length while the 14 remaining parameters were held constant at their optimal values. This analysis was independent of the magnitude of the parameter. The standard deviation of model predictions for velocity and run-length that resulted from changing a given parameter over this range of values was taken as a measure of the model's sensitivity to that parameter (see Fig. S2). It is important to note that velocity and run-length will have different rate-limiting steps and that these steps may shift to another step in the cycle depending on the substrate concentrations. Therefore, the sensitivity analysis was performed for various experimental conditions.

TABLE 1 Estimated parameter ranges and values used in the model prediction

Parameters (units)	Stage No. 1 search range	Stage No. 2 starting value	Final optimal parameter value	Literature range (Ref.)
k_1 (s^{-1})	3–750	4.6	6	>250 (4)
k_2 (s^{-1})	3–750	337	294	>250 (4)
k_3 (s^{-1})	3–750	663.7	1323	>250 (4)
k_{-D1} (s^{-1})	3–25	9.5	9.2	12–16 (4,14,45)
k_{-D2} (s^{-1})	3–25	21.4	27.3	29.5 (14)
k_{T1} ($\mu M^{-1}\ s^{-1}$)	0.15–2	1.6	0.15	0.9–1.6 (4,24)
k_{T2} ($\mu M^{-1}\ s^{-1}$)	0.15–2	1.24	0.42	0.9–1.6 (4,24)
k_{term1} (s^{-1})	0–30	0.51	0.47	N/d
k_{term2} (s^{-1})	0–30	0.07	0	N/d
k_{term3} (s^{-1})	0–30	5.6	75	N/d
k_{-1} ($\mu M^{-1}\ s^{-1}$)	0–0.5	0.29	0.00004	N/d
k_{-2} ($\mu M^{-1}\ s^{-1}$)	0–0.5	0.44	0.023	N/d
k_{-3} ($\mu M^{-1}\ s^{-1}$)	0–0.5	0.0003	0	N/d
k_{+D1} ($\mu M^{-1}\ s^{-1}$)	0–20	5.35	48.7	4–13 (4,6)
k_{+D2} ($\mu M^{-1}\ s^{-1}$)	0–20	17.6	4.7	4–13 (4,6)

RESULTS

The dependence of myosin Va velocity and run-length on [ATP], [ADP], and [P_i]

The velocity of single myosin Va motors increased, going from 10 μM to 10 mM ATP (Fig. 2 *a*, *circles*), consistent with previous studies (16). These data were fitted to the Michaelis-Menten equation (fits not shown), giving a V_{max} of 0.48 $\pm$ 0.01 μm/s and a K_m of 36 $\pm$ 3 μM. We repeated these observations in the presence of 40 mM P_i; this concentration was chosen to provide a definitive effect and for comparison with previous studies (16,19). Under this condition a similar dependence of velocity on ATP was observed (Fig. 2 *a*, *triangles*), but with a modest decrease in V_{max} (0.42 $\pm$ 0.01 μm/s) and a larger K_m (60 $\pm$ 5 μM).

In the absence of P_i, run-length decreased by as much as 50% with increasing ATP (Fig. 2 *b*, *circles*). This reduction in run-length suggests that with elevated ATP concentrations, a mechanochemical state prone to run termination is populated. Because the run-length does not decay to zero, an alternate biochemical pathway exists that is less prone to termination. In the presence of 40 mM P_i, the observed run-length was reduced and invariant at all concentrations of ATP characterized (Fig. 2 *b*, *triangles*). Since the run-length at high [ATP] is approximately the same as at high [P_i], this suggests an identical detachment pathway is populated.

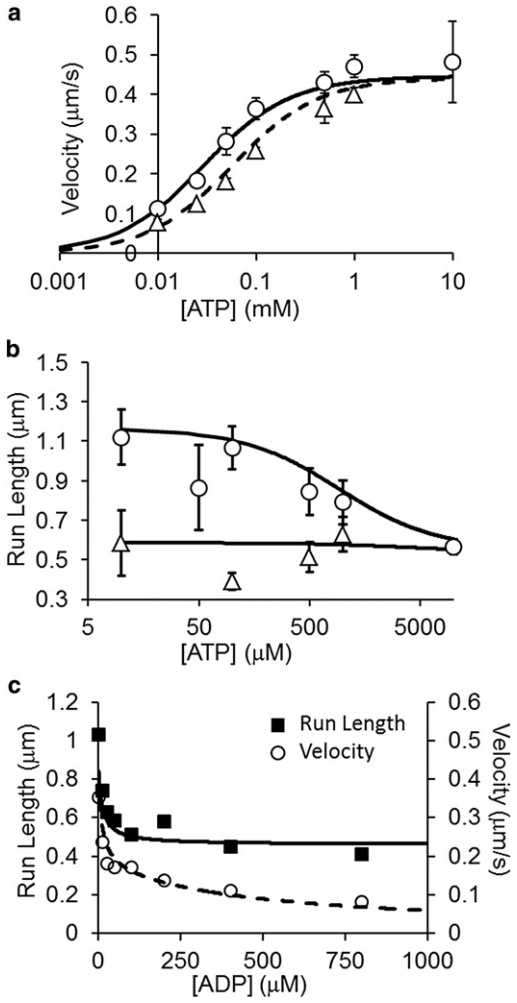

FIGURE 2 Effects of ATP, ADP, and P_i on myosin Va's velocity and run-length. For all plots, the solid line overlays are model-generated curves using the optimal parameter set from Table 1. (*a*) Myosin Va velocity is plotted as mean ± SE versus on a logarithmic [ATP] scale in the absence (*circles*) and presence (*triangles*) of 40 mM P_i. (*b*) Characteristic run-length constants derived from fits to cumulative frequencies (Fig. S1) are plotted as mean ± SE in the absence (*circles*) and presence (*triangles*) of 40 mM P_i on a logarithmic [ATP] scale. (*c*) (*Circles* and *squares*) Velocity and run-length, respectively, of myosin Va in 1 mM ATP versus [ADP].

To ensure that the labeling strategy used here had no effect on the motile properties of myosin Va, we repeated the ADP effects of a previous study (16) with Qdot-labeled myosin Va. It is clear from Fig. 2 *c* that increasing ADP reduces the run-length and velocity of myosin Va. The run-length was seen to form an asymptote from ~250 μM ADP, consistent with previous observations (16).

Model optimization, sensitivity, and predictions

The velocity and run-length data described above served as experimental constraints to globally optimize the 15 forward and reverse rate constants (i.e., parameters) of the mechanochemical model (Fig. 1). All of the trend curves shown in Fig. 2 are based on the optimal parameters in Table 1. As a whole, the data are fit remarkably well; the predicted rate constants are in good agreement with those reported in the literature from solution studies (4,14), with the exception of P_i release from the state 1 (k_1), which was considerably slower in our model (see Discussion). At 1 mM ATP and without added ADP or P_i, state 1 predominates due to the nearly similar rates of P_i release from the leading head and ADP release from the trailing head, with the exit from state 1 being rate-limiting for the entire cycle, as confirmed by sensitivity analysis (see Fig. S2 *b*).

Once the optimal model parameters were defined (Table 1), it was possible to predict the probability of the motor traveling down one of the three pathways, a major advantage over previous modeling efforts (16). The flux into each pathway is calculated as follows. At 0 mM [P_i], P_i release is irreversible, so the flux through path A equals $f_A = P_1 \times k_1$, the flux through path B equals $f_B = P_2 \times k_2$, and the flux through path C equals $f_C = P_3 \times k_3$. At 40 mM P_i, the optimal parameter values suggest that P_i rebinding is favored. As a result, the forward fluxes through the various paths at 40 mM P_i are as follows: path A, $f_A = P_1 \times k_1$; path B, $f_B = P_2 \times k_2 - P_5 \times k_{-2} \times [P_i]$; and path C, $f_C = P_3 \times k_3$.

As predicted by the model, without addition of ADP or P_i, myosin Va proceeds through all three pathways (Fig. 3 *a*). However, an increase in [ATP] shifts the flux from path B to path C. This explains the observed run-length reduction with increasing [ATP] (Fig. 2 *b*), because state 3 in path C offers the highest termination rate (k_{term3}, Table 1) since both heads are weakly bound. This was also evident in the sensitivity analysis: at 1 mM ATP, the run-length is sensitive to both k_{term1} and k_{term3}; however, at 10 mM ATP the model becomes most sensitive to k_{term3} and k_3, reflecting the increased probability of termination from state 3 (see Fig. S2, *b* and *c*). Due to surface immobilization of actin, the observed run-lengths under all conditions are likely to be underestimated as the motor is prevented from spiraling around the actin filament (22,23). If so, then these termination rates may be overestimated.

At 40 mM P_i, due to mass action, our modeling indicates that the forward flux through path B is greater due to limited passage to state 5, resulting in greater flux now passing through path C (Fig. 3 *b*). As the [ATP] is raised, additional flux is diverted to path C from path B while path A is unaffected. In addition, this model predicts the observed decrease in velocity and run-length with increasing [ADP] (see Fig. 2 *c*) at 1 mM ATP. As [ADP] increases, both path B and path C, which require ADP release from the trailing head of state 1, become inhibited (Fig. 3 *c*). Therefore passage out of state 1 is slowed, increasing the probability of detachment due to k_{term1}, which although slow (0.5 s^{-1}) accounts for the reduced run-length and the model being exquisitely sensitive to k_{term1} (see Fig. S2 *g* (*red bars*)). The velocity decrease is also expected due to the motor traveling predominantly down path A, which has a slowed rate

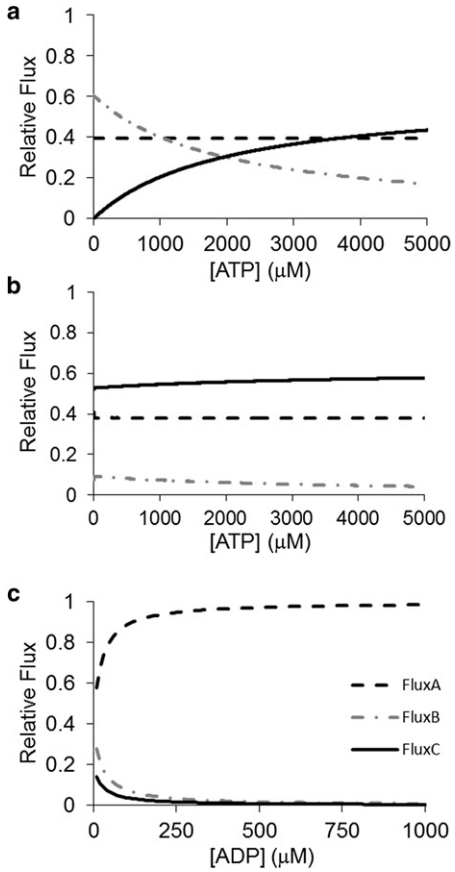

FIGURE 3 Biochemical flux distributions through the three paths of the branched model from Fig. 1. (Note that the figure legend in panel *c* pertains to all three graphs.) (*a*) In the absence of P_i, as the concentration of ATP is raised, flux is diverted along path *C*. (*b*) However, in the presence of 40 mM P_i there is little effect of ATP, indicating there are no competing pathways to path *C*. (*c*) At 1 mM ATP in the absence of P_i, the flux is seen to favor path *A* as the concentration of ADP is raised. For absolute flux values, see Fig. S5.

of passage. Sensitivity analysis indicates this is due to its slow P_i release rate (k_1) from the leading head in state 1 and the reduced rate of transition from state 5 to state 6, resulting from ADP rebinding (k_{+D2}) outcompeting ATP binding (k_{T2}) to the trailing head of state 5 (see Fig. S2 *g* (*blue bars*)).

Myosin Va stepping dynamics

To gain greater insight into the molecular basis for the observed changes in velocity and run-length, we characterized the motor's stepping dynamics (i.e., the step size and dwell time) under specific conditions. At 3 μM ATP, individual steps of the Qdot-labeled myosin Va head were easily resolved in both the presence and absence of 40 mM P_i (Fig. 4). The average forward step size was found to be 69 $\pm$ 1 nm in the absence of P_i (Fig. 4 *a*) and 67 $\pm$ 1 nm with 40 mM P_i (Fig. 4 *b*), consistent with only one of the two heads being Qdot-labeled and in agreement with previously reported step sizes (3,5,7,8). If both heads were

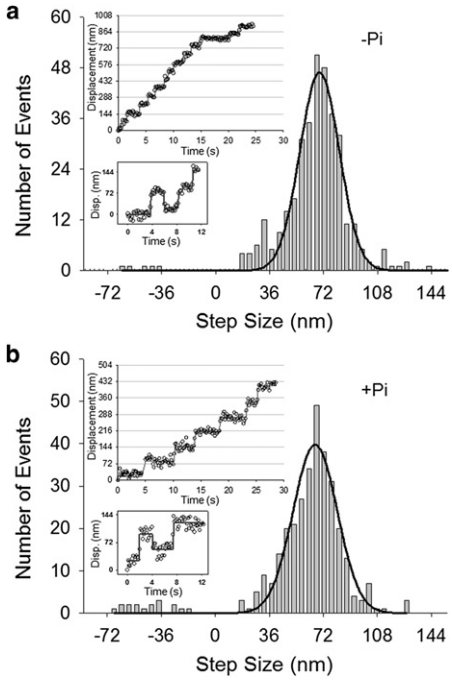

FIGURE 4 Effects of P_i on myosin Va's stepping dynamics. Individual myosin Va-Qdot steps within a run, highlighting forward steps and back steps (see *insets*) in the (*a*) absence of P_i, where the average size of forward steps is 69 $\pm$ 1 nm with a back-step/forward-step of 1.4%; and in the (*b*) presence of 40 mM P_i where the average step size of forward steps is 67 $\pm$ 1 nm, with a back-step/forward-step increased to 5.1%.

labeled, the point spread function of the individual Qdots would overlap and steps, if detected, would be ~36 nm, equivalent to the displacement of the motor's center of mass, which was not the case. In the absence of P_i, backsteps occurred infrequently (1.4%) but increased substantially to 5.1% upon addition of 40 mM P_i (Fig. 4). Given that the absolute number of backsteps was small, it was difficult to estimate the exact backstep amplitude.

With only one head being labeled, the observed dwell time is the sum of the sequential dwells for the steps of the labeled and unlabeled head. Assuming the stepping rates of the two heads are the same, we determined this rate (k) by fitting the histogram of dwell times (t) to the function $y = Atk^2e^{-kt}$ (7), resulting in a stepping rate of $k = 0.85 \pm 0.06\ s^{-1}$ at 3 μM ATP and 0 mM P_i, slowing to $0.61 \pm 0.03\ s^{-1}$ in the presence of 40 mM P_i (see Fig. S4), as would have been predicted based on the observed slowing of velocity (Fig. 2 *a*).

DISCUSSION

The processive movement of the molecular motor myosin Va provides a unique opportunity to correlate the stepping dynamics of a single molecule with its underlying biochemical and mechanical transitions. To probe these mechanochemical transitions, we characterized the effect of substrate concentration (ATP, ADP, P_i) on the velocity,

run-length, and individual steps taken by a single myosin Va under unloaded conditions. We have found, by using a free-fitting chemical kinetic description, that the minimal scheme required to explain the motor's processive properties is a branched set of kinetic pathways.

From this approach, individual forward and reverse rate constants were predicted for every biochemical transition. This provides a near-complete unloaded mechanochemical description of myosin Va processivity as well as a number of critical aspects of the motor's function. For example, myosin Va processivity is maintained under varying substrate conditions by the motor shifting between kinetic pathways and thus populating alternate states in its network of biochemical states. Additionally, the effects of intramolecular strain between the two heads is predicted, which appears to affect every transition involving substrate binding and release. Finally, the model provides an explanation to help reconcile the rates of P_i release observed at the ensemble level from solution biochemical studies with those inferred from these single-molecule experiments. These new insights go beyond our original and far less detailed kinetic model described in Baker et al. (16).

Substrate biases myosin Va's mechanochemical flux through multiple kinetic pathways

Consistent with what has been found in previous studies (16), myosin Va's ATP velocity dependence is hyperbolic. This relationship can be fit by a simple linear kinetic scheme, equivalent to path *A* in our model (Fig. 1), where ATP-binding to the trailing head of state 5 becomes rate-limiting at lower ATP concentrations (see Fig. S2 *a* and Fig. S3 *a*). However, at high ATP concentrations ($\geq$1 mM), a significant departure from expected behavior was seen: an ATP-induced reduction in run-length. This is not predicted for a linear scheme because changing ATP should only affect the rate of the cycle and not the rate of the termination step (see the Supporting Material). Therefore, at least one more pathway is required. Even though we had previously proposed a second pathway (path *B*, Fig. 1) to explain the effects of ADP on velocity and run-length (16), the addition of this pathway does not account for the observed run-length reduction with increasing ATP. Thus, as we previously speculated, a third critical pathway (path *C*) (16), is required so that ATP binding to the trailing head of state 2 results in a weakly bound complex (state 3) that is termination-prone.

The effect of high P_i concentrations on the velocity and more importantly, run-length also supports a branched kinetic model. If we assume a simple linear model once again, such as path *A*, the presence of P_i should prevent the leading head of state 1 from binding strongly to actin, substantially reducing the motor's stepping rate and thus velocity (see the Supporting Material). However, with both the stepping rate of the motor measured directly from the Qdot-labeled head (see Fig. S4) and the velocity (Fig. 2 *a*) decreasing by no more than ~20% in the presence of 40 mM P_i, a separate pathway must exist (path *C*) where addition of 40 mM P_i has little effect on velocity.

With the effect of substrate on myosin Va processivity best explained by a branched kinetic model, it is then possible to follow the flux through the various pathways (Fig. 3), which highlights the predictive strength of this model. For example, at physiological ATP (1 mM) in the absence of added ADP and P_i, the motor exists predominantly in state 1, where the trailing head is strongly bound and the leading head has yet to undergo its powerstroke (see Fig. S3 *a*). From this state, the motor either travels along the various pathways (Fig. 3 *a*: path *A*, 40%; path *B*, 40%; path *C*, 20%) or terminates its run (k_{term1}, Fig. 1). Because the flux out of state 1 is not dependent on ATP concentration, even at 10 mM ATP the motor maintains a constant flux of 40% along path *A*. The remaining 60% that normally travels through both paths *B* and *C* is shifted to path *C* because ATP binding to the trailing head outcompetes P_i release from the leading head of state 2. The resultant effect is the observed reduction in run-length at high ATP (Fig. 2 *b*), due to the increased probability of occupying the weakly bound state 3 from which run termination is more likely.

However, population of this weakly bound state is not fatal for processivity because the affinity of myosin Va's weak actin binding states are significantly greater than that of the class II myosins. This is due to the electrostatic interactions of the charged surface loop 2 (24). Therefore, successful processivity through state 3 is the result of a rate competition between rapid P_i release (k_3) from the leading head relative to termination (k_{term3}). Next, the reduced run-length in the presence of 40 mM P_i can be explained by a similar mechanism. Elevated P_i shifts the state 5-2 equilibrium toward state 2 (see Fig. S3 *b*), which results in a diversion of flux to path *C* (Fig. 3 *b*) and the subsequent population of the termination-prone state 3 at all ATP concentrations. Finally, the reduction in both run-length and velocity with the addition of ADP can be explained by ADP rebinding into the trailing head of the predominant state 1, leaving P_i release from the leading head the only option (i.e., path *A*) and effectively shutting down paths *B* and *C* (Fig. 3 *c*). With this scenario, the longer the time spent in state 1, the higher the risk of termination, and thus the reduction in run-length with increasing ADP (Fig. 2 *c*, *squares*). In addition, velocity slows as the predominant rate-limiting state becomes P_i release from the leading head of state 1 (k_1) coupled with equilibrium ADP release from state 4.

Intramolecular strain: a critical component of myosin Va gating and pathway selection

Load, applied either externally or originating from internal strain, plays a significant role in modulating the mechanochemistry of myosin Va (11,12,17,19,25). In this model,

which assumes no external load, intramolecular strain derived from the leading head attempting to or having performed its powerstroke is predicted to have significant effects on the rates of P_i release, ADP release, and ATP binding. It is important to note that these apparent strain dependencies were an outcome of the model and not assumed in any way (see Materials and Methods), further highlighting the importance of the combined experimental and modeling approach.

The model is presently limited to processivity under unloaded conditions and may require additional states that are only mechanically expressed under load (17,19). In addition, the model assumes that every ATPase cycle is coupled to a forward 72-nm displacement of the trailing head, which does not take into account the presence of altered intramolecular strain that might occur if the two heads were attached to actin at distances other than 36-nm apart (12,15,26).

ADP release

Probably the most critical step in which intramolecular strain gates the two heads of the myosin Va, biasing it to step forward, is thought to be the rate-limiting ADP release step. Mechanically, this is associated with a further ~5-nm rotation, distinct from the main swing (~20 nm) of the lever arm. This ADP-release-associated substep has been shown to possess significant load dependence (11). To ensure that the trailing head detaches before the leading head, assistive load imposed by the leading head attempting to undergo its powerstroke may accelerate ADP release from the trailing head (11,12,14). Alternatively, the resistive load of the trailing head could slow ADP release from the leading head (13,27). In our model ADP release can occur only from the trailing head of either state 1 or state 4. From state 1, the ~9 s^{-1} ADP release rate (k_{-D1}) is similar to that estimated for an unloaded motor (4), which is reasonable because the trailing head should not experience any physical constraints from the weakly bound leading head.

After P_i release (k_1), the leading head attempts its powerstroke, creating intramolecular strain between the two heads, both of which have ADP in the active site (state 4). If ADP release were to occur at any significant rate from the leading head (state 4), one would expect a loss in the motor's forward stepping bias and the appearance of backsteps. Because the probability of a backstep is extremely low under unloaded conditions, as observed here (Fig. 4) and previously (19,26), we set ADP release to 0 s^{-1}. This is consistent with very low rates of ADP release reported for the leading head (13,27). Based on this assumption, ADP release from the trailing head in state 4 is accelerated ($k_{-D2} \sim 27\ s^{-1}$), due to the assistive load generated by the attempted powerstroke of the leading head. This value is in very good agreement with that found in solution studies (14), and indicates that gating is achieved by an enhanced ADP release rate from the trailing head even when ADP release is prevented from the leading head. It is important to note that although we have here explained gating from the perspective of lever arm rotation, it may also occur through changes in myosin stiffness induced by nucleotide release.

ATP binding

With ADP release from the active site being sensitive to intramolecular strain, it is not surprising that ATP binding to the active site also shows sensitivity to strain. Specifically, ATP binding to the trailing head occurs either in state 2 or state 5, with the difference in intramolecular strain arising from whether ATP binds before (state 2) or after the leading head attempts its powerstroke (state 5). With the trailing head in state 5 experiencing an assistive load (Fig. 1), the model predicts that the rate of ATP binding, although lower than previously published values, does vary slightly (less than threefold) between the unassisted trailing head in state 2 ($k_{T1} = 0.15\ \mu M^{-1}\ s^{-1}$) and the assisted head in state 5 ($k_{T2} = 0.42\ \mu M^{-1}\ s^{-1}$).

This independent, modeling-based conclusion echoes single-molecule loading studies which also show a modest effect of load on the binding of ATP to myosin Va (11) and smooth muscle myosin II (28,29). Indeed, by using the measured load dependence of myosin Va (11), it is possible to estimate the strain required to generate our observed difference in k_T as 4.7 pN; this value is in accord with that (3.6 pN) estimated from a mechanical stiffness model (11). This has positive implications on processivity, where the lower rate of ATP binding to the trailing head of state 2 will favor P_i release from the leading head before ATP binding, accounting for the bias for the motor to take the less-termination-prone path *B* over path *C* below ~2 mM ATP (Fig. 3 *a*).

Phosphate release

P_i release is associated with one of the most critical steps in the motor's ATPase cycle: the transition from the weak to the strong-binding state and the powerstroke. From previous optical trap studies in which external load was applied to a single myosin Va motor, we showed that the release of P_i commits the motor to an extremely load-dependent, strongly bound state that must have ADP bound to both heads (19). However, without applying external load in this study, the P_i release rate defined in the model may encompass several transitions including P_i release itself followed by strong binding to actin and the powerstroke. Therefore, the modeled P_i release could exhibit sensitivity to load. From a specific state within each of the proposed pathways, P_i release can occur (path *A*, state 1; path *B*, state 2; and path *C*, state 3; see Fig. 1).

Interestingly, the P_i release rate from each of these three states differs substantially due to varying levels of intramolecular strain. This strain arises as the leading head binds to actin after its diffusive search (11,30,31) with the magnitude

of strain determined by the lever-arm rotation of the trailing head. Therefore, as strain is relieved within the motor, the P_i release rate from the leading head is predicted to progressively increase. Starting with the most internally strained state 1 ($k_1 = 6\ s^{-1}$) , this is followed by a reduction in strain due to a small 4.3-nm rotation of the trailing head's lever arm upon ADP release (11) in state 2 ($k_2 = 294\ s^{-1}$), with P_i release being very rapid ($k_3 = 1323\ s^{-1}$) from the least strained state 3, as the trailing head becomes weakly bound to actin upon ATP binding.

An alternate explanation for the increased P_i release from the leading head with differences in the nucleotide state of the trailing head is that P_i release could be limited by the diffusional search of the leading head (30,32). If so, the leading head's diffusional search distance would be greater in state 1 compared to either state 2 or state 3, again due to the additional lever-arm rotation either concomitant with or after ADP release.

As stated above, the predominant or waiting state predicted by the model is state 1 in the presence of 1 mM ATP and no added ADP and P_i (see Fig. S3 *a*). This occurs because the P_i release rate from the leading head (k_1) is comparable to the ADP release rate from the trailing head (k_{-D1}). This is contradictory to studies, which measured a fast P_i release rate ($>228\ s^{-1}$) compared to a much slower ADP release rate (12–16 s^{-1}) (4,14). However, the P_i release rate from myosin Va during processive movement has yet to be measured directly; instead these were inferred from solution studies using single-headed myosin Va S1 or from the initial encounter of the double-headed myosin Va HMM with actin. Knowing the flux distribution (Fig. 3 *a*) through all three possible pathways, the overall P_i release rate should be a weighted average of 391 s^{-1}, which is in much better agreement with the literature values. Direct measurement of lead head binding has been shown to occur at 180 s^{-1} (30) and was not affected by $[P_i]$. This may be the weak association of the lead head (state 1), after which myosin Va can then go on to release P_i from the pathways described here. The differing rates of P_i release highlight the intricate sensitivity of this cargo transport molecule to load.

As internal strain is relieved with ADP release from the trailing head of state 1 or ATP binding to the trailing head of state 2, the strong binding and P_i release of the lead head is favored. This ensures that the biochemistry of the two heads remains asynchronous and processivity maintained. P_i rebinding within the model does not follow this systematic load-dependence. The role of rebinding is important for understanding how P_i may affect run-lengths and velocity, because this would provide an alternate detachment route in high P_i from state 1 (equivalent to state 6). However, the predicted absence of P_i rebinding (k_{-3}) to state 6 would suggest that the existence of such a detachment pathway is unlikely; this may indicate that internal load is required for P_i to rebind as in states 4 and 5. A significant energy barrier to reversal of the lever arm has been recently suggested using direct imaging of the postpower-stroke recovery upon binding ATP (21).

Phosphate increases backstep probability

Unloaded myosin Va rarely takes a backstep, but with resistive load the probability increases substantially (17,19, 26,33), eventually equaling the probability of taking a forward step at stall forces. In a recent study (26), load was applied to an N-terminal Qdot-labeled motor using a laser trap, and backsteps were found to be a true reversal of the motor's hand-over-hand stepping pattern. Here we confirm that in the absence of load, the backstep to forward step probability is extremely low (~1%) and that the addition of 40 mM P_i increased this probability nearly fivefold (i.e., 5%), as previously observed (19). This relatively low percentage may be due to the forward bias provided by the lead head adopting a postrecovery conformation after ATP hydrolysis (21). Although backsteps are not an explicit aspect of the model, by mass action, elevated P_i shifts the flux to path *C*, where the leading head in states 1 and 2 would be trapped in a weak binding state, increasing the chance of a backstep due to thermal energy. This would result in a decrease in the apparent velocity of stepping and also increase the chances of detachment, thus potentially reducing run-length. From a cellular perspective, regardless of whether P_i was elevated or not, the ability of myosin Va to step backward and then restart its processive run would permit the motor to negotiate objects blocking its path, thus ensuring successful cargo delivery.

Comparison with similar models

A number of models have been proposed to describe the large number of structural and mechanical features of myosin Va (15,34–38). Earlier linear models (5,14) describe a single biochemical pathway for the generation of motion, with branches off the main pathway leading to the detachment of myosin Va and run termination. Although simple, these models are unable to accurately predict the reduction in run-length due to ADP and P_i binding. Chemical kinetic models are essential to link the known biochemistry to the observed mechanics of myosin Va motion. A series of such models, based initially on observed data (16,17) to more recent theoretical-only studies, offer valuable insight into the internal (18) and externally loaded (39) mechanochemical cycles.

Here we discuss two mechanochemical models most relevant to this study proposed by Bierbaum and Lipowsky (39) and Wu et al. (18) and their ability to predict the effects of substrate on velocity and run-length. First, Bierbaum and Lipowsky (39) generate a complete network description of motor states with each head containing ATP, ADP, or being empty (i.e., nucleotide-free) as a function of position along the actin filament. Due to the complexity of this network, which included nine states and 18 chemical reactions at

each actin position, Bierbaum and Lipowsky simplified this network to one containing only six chemical transitions in an effort to reduce the model's parameter space and to focus on the load dependence of nucleotide binding to the leading head.

In effect, this model becomes a linear kinetic scheme for forward stepping as proposed previously (5). This linearity defines the primary difference with our model, and as a result there are no alternate pathways to provide for the reduction in run-length with elevated ATP, which our model predicts successfully (Fig. 2 *b*). Another example would be that there is no provision in the Bierbaum and Lipowsky model (39) for an ADP.P_i state with P_i release being load-dependent. As a result, their model predicts a strong inhibition of velocity at only 1 mM P_i, in contrast to the data presented here, which experimentally demonstrates only a marginal effect on the motor's velocity even at 40 mM P_i (Fig. 2 *a*).

Wu et al. (18) take a similar approach to that outlined in our study, proposing a branched triple pathway model to explain the presence of 12-nm substeps whose lifetime was neither ATP- nor ADP-dependent, which are then followed by a 24-nm main step (17), a phenomenon previously predicted by a stochastic discrete model (38). To model these data, Wu et al. (18) proposed a new state $T'D^w$ with an actin-detached rear ATP-bound head (T') and an ADP-bound weakly attached lead head (D^w) to generate a 12-nm substep. Their model fits assume state transition rates from the literature rather than relying on best global fits as described here. As a result, their model falls short in predicting the significant reduction in run-length with increasing ADP (Fig. 2 *c*) and at high [ATP].

Our approach of combining experiment and theory offers a new, to our knowledge, understanding of internal strain and its effects on transition rate kinetics. By coupling our approach with an elastic mechanical model description (15,36), there is an opportunity for a unified model in the presence and absence of external load that could also account for substeps. Finally, we introduce a rigorous approach to fitting available data to a chemical kinetic model using an iterative and unbiased parameter search method rather than relying solely on literature-based values.

CONCLUSIONS

Here we have developed a mechanochemical model of myosin Va motility using the rigorous and objective approach of fitting an explicit set of differential equations that describe the model. The branched kinetic scheme thus derived describes the dependence of velocity and run-length on varying substrate concentrations under unloaded conditions. Specifically, during processive movement and cargo transport, myosin Va can take one of at least three mechanochemical pathways per step. Each of the biochemical transitions were found to possess load dependences that were generated by internal strain, opening the door for future investigations that probe the effect of external loads on myosin Va stepping dynamics.

Therefore, navigation through these biochemical pathways is governed by the prevailing conditions, permitting myosin Va to adjust its cargo transport mechanism by simply switching gears to accommodate intracellular variations in biochemical conditions and physical constraints. For example, changes in the cell's metabolic state could alter concentrations of ATP and its hydrolysis products, ADP and P_i, any of which can have profound effects on myosin Va processivity. Physiologic intracellular nucleotide concentrations vary within and across tissue types such that ADP concentrations can attain μM levels (40–43) while ATP also varies with ~3 mM in the brain and higher levels estimated in skeletal muscle (43,44).

With substantial redundancy in its hydrolytic and mechanical pathways that offer alternatives when necessary, myosin Va appears to be well suited for the challenges of the intracellular milieu.

SUPPORTING MATERIAL

One table, six figures, and references (46–49) are available at http://www.biophysj.org/biophysj/supplemental/S0006-3495(12)00809-0.

We thank the Trybus Laboratory for the expressed myosin Va, S. Beck for technical assistance, G. Kennedy (University of Vermont Instrumentation and Model Facility) for optomechanics expertise, T. Ashikaga (University of Vermont Biometry Facility) for suggestions on how to derive an optimal fit to a multiparameter model, Drs. C. Danforth and D. Bentil (University of Vermont Department of Mathematics) for the algorithm and assistance in solving the state equations, Dr. S. Walcott for help with MATLAB, and the Warshaw Lab for numerous discussions.

This work was supported by funds from the National Institutes of Health to D.M.W. (HL059408 and GM094229), the American Heart Association to M.Y.A. (12SDG11930002), and N.M.K. is supported by the Biotechnology and Biological Sciences Research Council (BB/I003460/1).

REFERENCES

1. Reck-Peterson, S. L., D. W. Provance, Jr., …, J. A. Mercer. 2000. Class V myosins. *Biochim. Biophys. Acta.* 1496:36–51.
2. Vale, R. D. 2003. The molecular motor toolbox for intracellular transport. *Cell.* 112:467–480.
3. Mehta, A. D., R. S. Rock, …, R. E. Cheney. 1999. Myosin-V is a processive actin-based motor. *Nature.* 400:590–593.
4. De La Cruz, E. M., A. L. Wells, …, H. L. Sweeney. 1999. The kinetic mechanism of myosin V. *Proc. Natl. Acad. Sci. USA.* 96:13726–13731.
5. Rief, M., R. S. Rock, …, J. A. Spudich. 2000. Myosin-V stepping kinetics: a molecular model for processivity. *Proc. Natl. Acad. Sci. USA.* 97:9482–9486.
6. Trybus, K. M., E. Krementsova, and Y. Freyzon. 1999. Kinetic characterization of a monomeric unconventional myosin V construct. *J. Biol. Chem.* 274:27448–27456.
7. Yildiz, A., J. N. Forkey, …, P. R. Selvin. 2003. Myosin V walks hand-over-hand: single fluorophore imaging with 1.5-nm localization. *Science.* 300:2061–2065.

8. Warshaw, D. M., G. G. Kennedy, …, K. M. Trybus. 2005. Differential labeling of myosin V heads with quantum dots allows direct visualization of hand-over-hand processivity. *Biophys. J.* 88:L30–L32.
9. Sellers, J. R., and C. Veigel. 2006. Walking with myosin V. *Curr. Opin. Cell Biol.* 18:68–73.
10. Forgacs, E., T. Sakamoto, …, H. D. White. 2009. Switch 1 mutation S217A converts myosin V into a low duty ratio motor. *J. Biol. Chem.* 284:2138–2149.
11. Veigel, C., S. Schmitz, …, J. R. Sellers. 2005. Load-dependent kinetics of myosin-V can explain its high processivity. *Nat. Cell Biol.* 7:861–869.
12. Purcell, T. J., H. L. Sweeney, and J. A. Spudich. 2005. A force-dependent state controls the coordination of processive myosin V. *Proc. Natl. Acad. Sci. USA.* 102:13873–13878.
13. Sakamoto, T., M. R. Webb, …, J. R. Sellers. 2008. Direct observation of the mechanochemical coupling in myosin Va during processive movement. *Nature.* 455:128–132.
14. Rosenfeld, S. S., and H. L. Sweeney. 2004. A model of myosin V processivity. *J. Biol. Chem.* 279:40100–40111.
15. Vilfan, A. 2005. Elastic lever-arm model for myosin V. *Biophys. J.* 88:3792–3805.
16. Baker, J. E., E. B. Krementsova, …, D. M. Warshaw. 2004. Myosin V processivity: multiple kinetic pathways for head-to-head coordination. *Proc. Natl. Acad. Sci. USA.* 101:5542–5546.
17. Uemura, S., H. Higuchi, …, S. Ishiwata. 2004. Mechanochemical coupling of two substeps in a single myosin V motor. *Nat. Struct. Mol. Biol.* 11:877–883.
18. Wu, Y., Y. Q. Gao, and M. Karplus. 2007. A kinetic model of coordinated myosin V. *Biochemistry.* 46:6318–6330.
19. Kad, N. M., K. M. Trybus, and D. M. Warshaw. 2008. Load and P_i control flux through the branched kinetic cycle of myosin V. *J. Biol. Chem.* 283:17477–17484.
20. Kerssemakers, J. W., E. L. Munteanu, …, M. Dogterom. 2006. Assembly dynamics of microtubules at molecular resolution. *Nature.* 442:709–712.
21. Shiroguchi, K., H. F. Chin, …, K. Kinosita, Jr. 2011. Direct observation of the myosin Va recovery stroke that contributes to unidirectional stepping along actin. *PLoS Biol.* 9:e1001031.
22. Ali, M. Y., S. Uemura, …, S. Ishiwata. 2002. Myosin V is a left-handed spiral motor on the right-handed actin helix. *Nat. Struct. Biol.* 9: 464–467.
23. Arsenault, M. E., Y. Sun, …, Y. E. Goldman. 2009. Using electrical and optical tweezers to facilitate studies of molecular motors. *Phys. Chem. Chem. Phys.* 11:4834–4839.
24. Yengo, C. M., E. M. De la Cruz, …, H. L. Sweeney. 2002. Kinetic characterization of the weak binding states of myosin V. *Biochemistry.* 41:8508–8517.
25. Veigel, C., F. Wang, …, J. E. Molloy. 2002. The gated gait of the processive molecular motor, myosin V. *Nat. Cell Biol.* 4:59–65.
26. Lu, H., G. G. Kennedy, …, K. M. Trybus. 2010. Simultaneous observation of tail and head movements of myosin V during processive motion. *J. Biol. Chem.* 285:42068–42074.
27. Forgacs, E., S. Cartwright, …, H. D. White. 2008. Kinetics of ADP dissociation from the trail and lead heads of actomyosin V following the power stroke. *J. Biol. Chem.* 283:766–773.
28. Veigel, C., J. E. Molloy, …, J. Kendrick-Jones. 2003. Load-dependent kinetics of force production by smooth muscle myosin measured with optical tweezers. *Nat. Cell Biol.* 5:980–986.
29. Kad, N. M., J. B. Patlak, …, D. M. Warshaw. 2007. Mutation of a conserved glycine in the SH1-SH2 helix affects the load-dependent kinetics of myosin. *Biophys. J.* 92:1623–1631.
30. Dunn, A. R., and J. A. Spudich. 2007. Dynamics of the unbound head during myosin V processive translocation. *Nat. Struct. Mol. Biol.* 14:246–248.
31. Ali, M. Y., E. B. Krementsova, …, D. M. Warshaw. 2007. Myosin Va maneuvers through actin intersections and diffuses along microtubules. *Proc. Natl. Acad. Sci. USA.* 104:4332–4336.
32. Shiroguchi, K., and K. Kinosita, Jr. 2007. Myosin V walks by lever action and Brownian motion. *Science.* 316:1208–1212.
33. Clemen, A. E., M. Vilfan, …, M. Rief. 2005. Force-dependent stepping kinetics of myosin-V. *Biophys. J.* 88:4402–4410.
34. Craig, E. M., and H. Linke. 2009. Mechanochemical model for myosin V. *Proc. Natl. Acad. Sci. USA.* 106:18261–18266.
35. Skau, K. I., R. B. Hoyle, and M. S. Turner. 2006. A kinetic model describing the processivity of myosin-V. *Biophys. J.* 91:2475–2489.
36. Lan, G., and S. X. Sun. 2005. Dynamics of myosin-V processivity. *Biophys. J.* 88:999–1008.
37. Xie, P., S. X. Dou, and P. Y. Wang. 2006. Model for kinetics of myosin-V molecular motors. *Biophys. Chem.* 120:225–236.
38. Kolomeisky, A. B., and M. E. Fisher. 2003. A simple kinetic model describes the processivity of myosin-v. *Biophys. J.* 84:1642–1650.
39. Bierbaum, V., and R. Lipowsky. 2011. Chemomechanical coupling and motor cycles of myosin V. *Biophys. J.* 100:1747–1755.
40. Mora, B., P. T. Narasimhan, …, P. B. Barker. 1991. 31P saturation transfer and phosphocreatine imaging in the monkey brain. *Proc. Natl. Acad. Sci. USA.* 88:8372–8376.
41. Brosnan, M. J., L. Chen, …, A. P. Koretsky. 1990. Free ADP levels in transgenic mouse liver expressing creatine kinase. Effects of enzyme activity, phosphagen type, and substrate concentration. *J. Biol. Chem.* 265:20849–20855.
42. Koretsky, A. P., M. J. Brosnan, …, T. Van Dyke. 1990. NMR detection of creatine kinase expressed in liver of transgenic mice: determination of free ADP levels. *Proc. Natl. Acad. Sci. USA.* 87:3112–3116.
43. Williams, S. P., A. M. Fulton, and K. M. Brindle. 1993. Estimation of the intracellular free ADP concentration by ^{19}F NMR studies of fluorine-labeled yeast phosphoglycerate kinase in vivo. *Biochemistry.* 32:4895–4902.
44. Veech, R. L., J. W. Lawson, …, H. A. Krebs. 1979. Cytosolic phosphorylation potential. *J. Biol. Chem.* 254:6538–6547.
45. Wang, F., L. Chen, …, J. R. Sellers. 2000. Effect of ADP and ionic strength on the kinetic and motile properties of recombinant mouse myosin V. *J. Biol. Chem.* 275:4329–4335.
46. Pardee, J. D., and J. A. Spudich. 1982. Purification of muscle actin. *Meth. Enzymol.* 85:164–181.
47. Gyimesi, M., B. Kintses, …, A. Málnási-Csizmadia. 2008. The mechanism of the reverse recovery step, phosphate release, and actin activation of *Dictyostelium* myosin II. *J. Biol. Chem.* 283:8153–8163.
48. Fabiato, A., and F. Fabiato. 1979. Calculator programs for computing the composition of the solutions containing multiple metals and ligands used for experiments in skinned muscle cells. *J. Physiol.* (*Paris*). 75: 463–505.
49. Ali, M. Y., H. Lu, …, K. M. Trybus. 2008. Myosin V and kinesin act as tethers to enhance each others' processivity. *Proc. Natl. Acad. Sci. USA.* 105:4691–4696.